Applied Journal of Environmental Engineering Science

Doping dependent on the p-type thermoelectric properties of ZnO: First principal calculation

Hassan Ahmoum[1,2,3,4], Guojian Li[1,], Yang Jin[1,2], Mourad Boughrara[3,*], Mohd Sukor Su'ait[4], Siddheshwar Chopra[5], D. P. Rai[6], Mohamed Kerouad[3], Qiang Wang[1]**

[1] *Key Laboratory of Electromagnetic Processing of Materials (Ministry of Education), Northeastern University, Shenyang, 110819, China*

[2] *School of Metallurgy, Northeastern University, Shenyang, 110819, China*

[3] *Laboratoire de Physique des Matériaux et Modélisation des Systémes (LP2MS), Unité Associée au CNRST-URAC: 08, Faculty of Sciences, University Moulay Ismail, B.P. 11201, Zitoune, Meknes, Morocco.*

[4] *Solar Energy Research Institute (SERI), the National University of Malaysia, 43600, Bangi, Selangor, Malaysia.*

[5] *Department of Physics, AIAS, Amity University, Noida, India*

[6]*Physical Sciences Research Center (PSRC), Department of Physics, Pachhunga University College, Aizawl 796001, India*.

Corresponding author. E-mail : Boughrara_mourad@yahoo.fr; gjli@mail.neu.edu.cn

Received 25 Nov 2020, Revised 13 Dec 2020, Accepted 28 Dec 2020

Abstract

First principles calculations were used to investigate the structural, electronic, dielectric, optical and thermoelectric properties of Cu-X (where X= C, N, S, F, P) doped ZnO films. In this work, density functional theory based on the generalized-gradient-approximation plus Hubbard parameters (GGA+U) and Boltzmann transport theory have been used to calculate the electronic and thermoelectric properties, respectively. It is concluded that the Cu-F co-doped ZnO is n-type semiconductor while the others are p-type semiconductors. All the simulated materials are found to be transparent in the visible region with varying values of the electronic band gap. Furthermore, Cu-S co-doped ZnO exhibits the best thermoelectric performance amongst all the other co-doped elements.

Keywords: *First Principle; P-type ZnO; Transmittance; Thermoelectric;*

1.0 Introduction

Optoelectronic devices such as photodiode, solar cells, light emitting diodes, optical fibers and laser diodes generally consist of P-N junctions [1-6]. Commonly used N-type semiconductors are GaN, SnO and ZnO which are used in different aforementioned applications [7]. Out of these, ZnO is extensively used because

of the favorable defects such as interstitial zinc and oxygen vacancy. Furthermore, it offers several advantages such as high availability, non-toxicity, and its higher stability (due to large exciton binding energy ~60 meV) [8]. Hetero-junction devices are based on two different type of materials which lead to lattice mismatching resulting in the dislocation at the interface which facilitates the trapping of charge carriers and hence deteriorating the device's life time [9, 10]. In order to improve the stability and device life time, it is preferable to fabricate homo-junction instead of the hetero-junction, which would passivate the defects that occurred from the dislocation at the interface [11].

The main challenge concerning zinc oxide is to produce a stable p-type ZnO due to the combination of self-compensating effect [12]. Many experimental and theoretical investigations on p-type ZnO have been reported [13-19]. Nitrogen is suggested to be a good ZnO dopant, but first principles calculations have shown that N has higher formation energy leading to unstable p-type ZnO [20]. Other elements like Li and Na have also been explored theoretically, and it is found that these elements prefer to occupy the interstitial position in the Wurtzite structure of ZnO and act as donors [9, 11]. Notably the mono-doping strategy has been found unfavorable to obtain stable p-type ZnO films. The co-doped method by using two acceptor elements ~~is~~ are found to be suitable for fabrication of a stable p-type ZnO [21]. Zhao et al. have investigated the K-N co-doped ZnO and have shown that shallow acceptor level becomes lower with dual acceptor doping, as compared to the mono-doping [22]. This is beneficial for obtaining a stable p-type ZnO.

Thermoelectric materials are known for their capability of transforming the waste heat into electricity [23-28]. But usage of these materials is limited by the low efficiency and high cost. Their efficiency is determined by a dimensionless value known as Figure of merit,

$$\mathrm{ZT} = \frac{\alpha^2 \sigma T}{k} \qquad (1)$$

Where α, σ, T and k are the Seebeck confficient, electrical conductivity, absolute temperature (in Kelvin) and thermal conductivity, respectively [10]. The term "$\alpha^2\sigma$" is the power factor. It has been reported that *p*-type ZnO materials demonstrate better thermoelectric (TE) properties than *n*-type ZnO due to the degeneracy occurring due to the combination of heavy and light bands [29]. Thus, ZnO semiconductor materials are a promising p-type conduction candidate for thermoelectric application.

In this present research work ~~investigation~~, we have presented a theoretical study based on the density functional theory on the Cu-(C, N, S, F, P) co-doped ZnO films and discuss the effects of different impurities on the structural, electronic, dielectric, optical and thermoelectric properties, respectively.

2.0 Computational Methods

In this work, the first-principles calculations were carried out using plane wave method, which is based on density functional theory (DFT) [30]. Exchange and correlation effects are treated under the generalized gradient approximation (GGA) within Perdew Burke Ehrenkof (PBE) functional [31]. All atomic coordinates and lattice parameters of ZnO were fully relaxed before calculating the structural, electronic,

dielectric, optical and thermoelectric properties. The plane-wave energy cutoff was chosen to be 450 eV. Monkhorst-Pack grid of 9×9×9 was employed for the geometry optimization and the self-consistent field (SCF) calculation [32]. The tolerance in the geometry optimization was set at 1×10^{-5} eV/atom and 1×10^{-6} eV/atom for the SCF calculation. The maximum force was 0.03 eV/Å. The GGA + U method was used to correct the band gap value of ZnO. The Hubbard (U) values (in "eV") employed in this work are U (d, Zn) = 10, U (p, O) = 7, [9, 11] respectively. All calculations were performed on the ZnO (2×2×2) super cell, which contains 16 atoms (O and Zn) in total.

3.0 Results and Discussion

3.1 Structural Properties

In **Table 1** we have presented the optimized lattice parameters of different supercells of ZnO co-doped Cu-(C, N, P, S and F). It is an evident that the lattice parameters of pure *ZnO* are in good agreement with the other experimental [33] and theoretical [34] results, confirming the reliability of the calculation method used in this study. It is well known that doping a semiconductor with electrically active atoms modifies the lattice parameters due to the size effect [9]. Therefore, here variation of the volume of different systems has also been explored. Knowingly, volume depends on the nature of different impurities. As it can been seen that the co-doped Cu-(N and C) leads to the reduced primitive cell volume. The origin of this behavior can be explained from the difference in the atomic radii between (Cu<Zn; C and N<O). However, for the rest of the doping elements (P, S, F), the increase in lattice parameters has been observed due to the difference in ionic radii as compared to O. Moreover, it has been observed that the incorporation of the different elements (P and S) result in the elongation of the lattice parameter *"c"*. Similar phenomena have also been reported in the recent work by W. Yu et al. where the effect of doping (C, N and S) on physical properties of ZnO was studied by ab-initio calculations [35].

Table 1 Structural properties of ZnO co-doped Cu-(C, N, P, S, F). "d" values are in Angstroms.

Model	Method	*a*/Å	*c*/Å	*V*/Å^3	*c*/a	d_{Zn-O}	d_{Cu-O}	d_{Zn-X}
Pure ZnO	This work	3.251	5.239	47.95	1.609		-	-
	Experimental [37]	3.252	5.208	47.70	1.601			
	Simulation [38]	3.248	5.222	47.71	1.608			
Cu:C-ZnO	This work	3.253	5.221	47.84	1.613	1.959	1.902	2.007
Cu:N-ZnO	This work	3.248	5.228	47.76	1.609	1.967	1.891	1.982
Cu:P-ZnO	This work	3.276	5.360	49.82	1.636	1.962	1.905	2.247
Cu:S-ZnO	This work	3.281	5.337	49.75	1.626	1.961	1.922	2.217
Cu:F-ZnO	This work	3.270	5.297	49.05	1.619	1.913	1.929	2.101

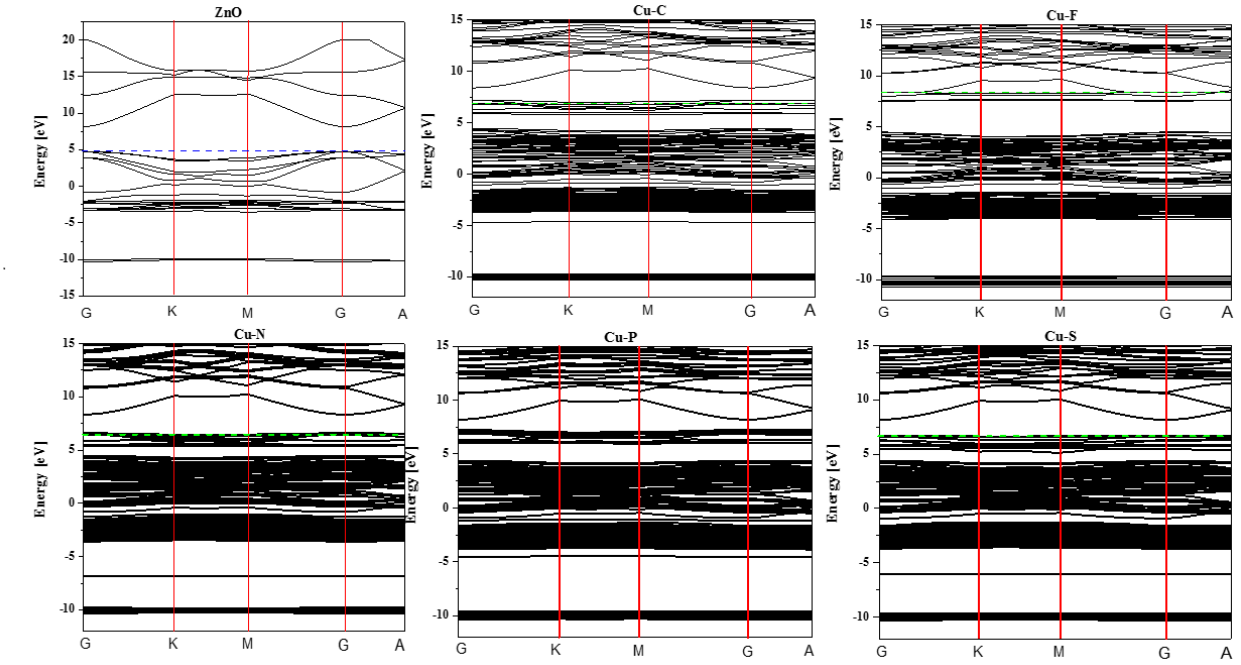

Figure 1. band structure of pure and codoped ZnO

3.2 Electronic Properties

Electronic properties hold an importance in understanding the various physical properties such as dielectric, optical and electrical respectively. In order to study the co-doping effect on the electronic properties, the electronic band structure and the partial density of states of pure and *Cu-(C, N, S, F, P)* co-doped *ZnO* have been calculated. The Fermi level is set at exact value (no shifting) in this study. Fig. 1 show the pure ZnO exhibit direct band gap because the maximum of the valence band and the minimum of the conduction band are both located at the center of the bouillon zone, the calculated band gap is found to be 3.38 eV which is in excellent accord with the experimental results measured by ultraviolet-visible-infrared spectroscopy and by the photoluminescence spectrum and this could be attributed to the Hubbard correction applied in this work [24]. For the codoped system is it found the presence an impurity band in the middle of the band gap except for the case of Cu-F codoped because in this last one, the material is finding to be a n-type degenerated semiconductor. For more information we have also calculated the partial density of states as shown in **Fig 2. a**. for pure ZnO it is found that the valence band is formed by the hybridization between 2p-O and 3d-Zn states and the conduction band is formed by 4s-Zn. In the Cu-F model, the semiconductor becomes n-type as the Fermi level gets shifted to the bottom of the conduction band. In addition, the 3d-Zn states are found to be hybridized with the 4s-Zn states to form the conduction band, while the valence band is formed by 2p-O and 2p-F as evident from **Fig. 2-b**. For the rest of the models *Cu-(C, N, S, and P)* a new impurity band is formed within in the band gap due to the hybridization between 3d-Cu-(2p-C, 2p-N, 2p-P and 3p-S) while the conduction band is still formed by the same states 4s-Zn states and the valence band is formed by 2p-O states as shown in **Fig. 2-c-f**.

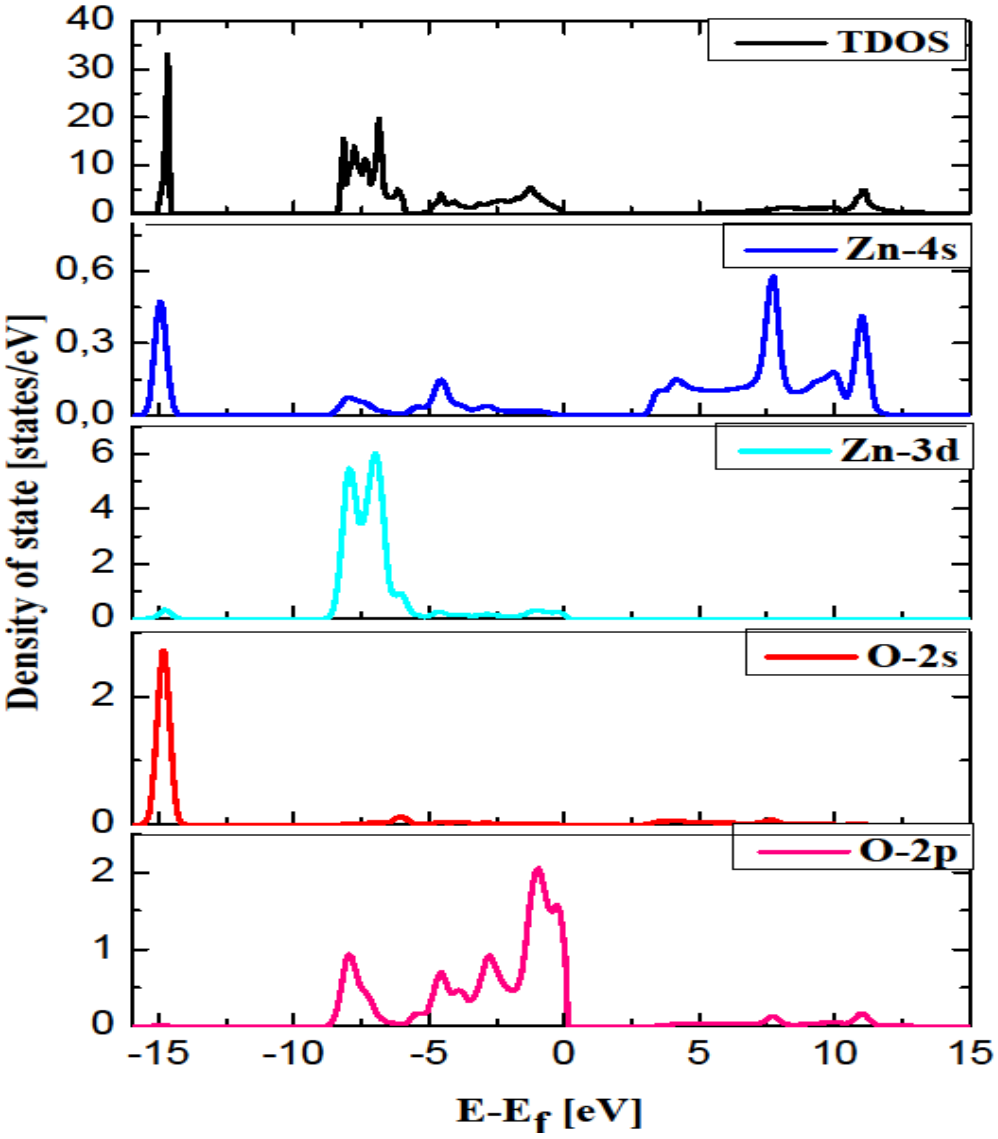

Figure 2-a: Partial density of states of pure ZnO

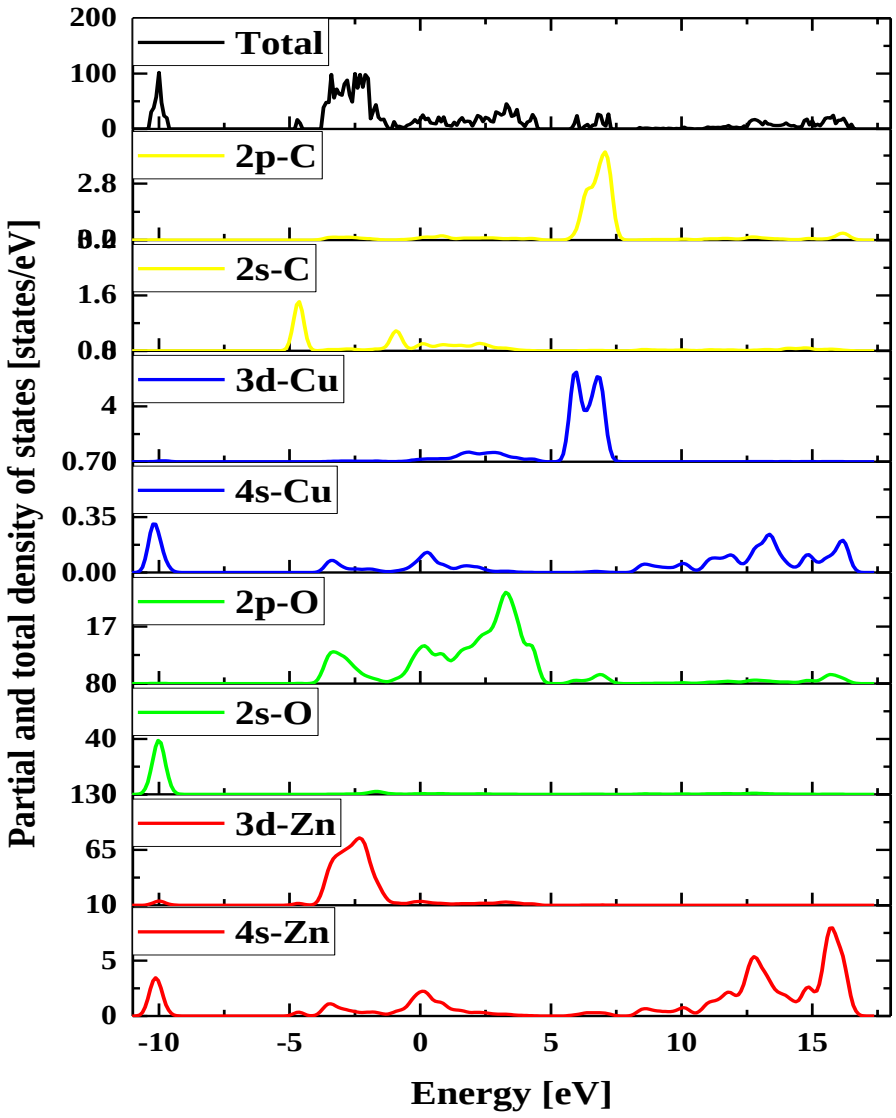

Figure 2-b: Partial density of states of Cu-C codoped ZnO

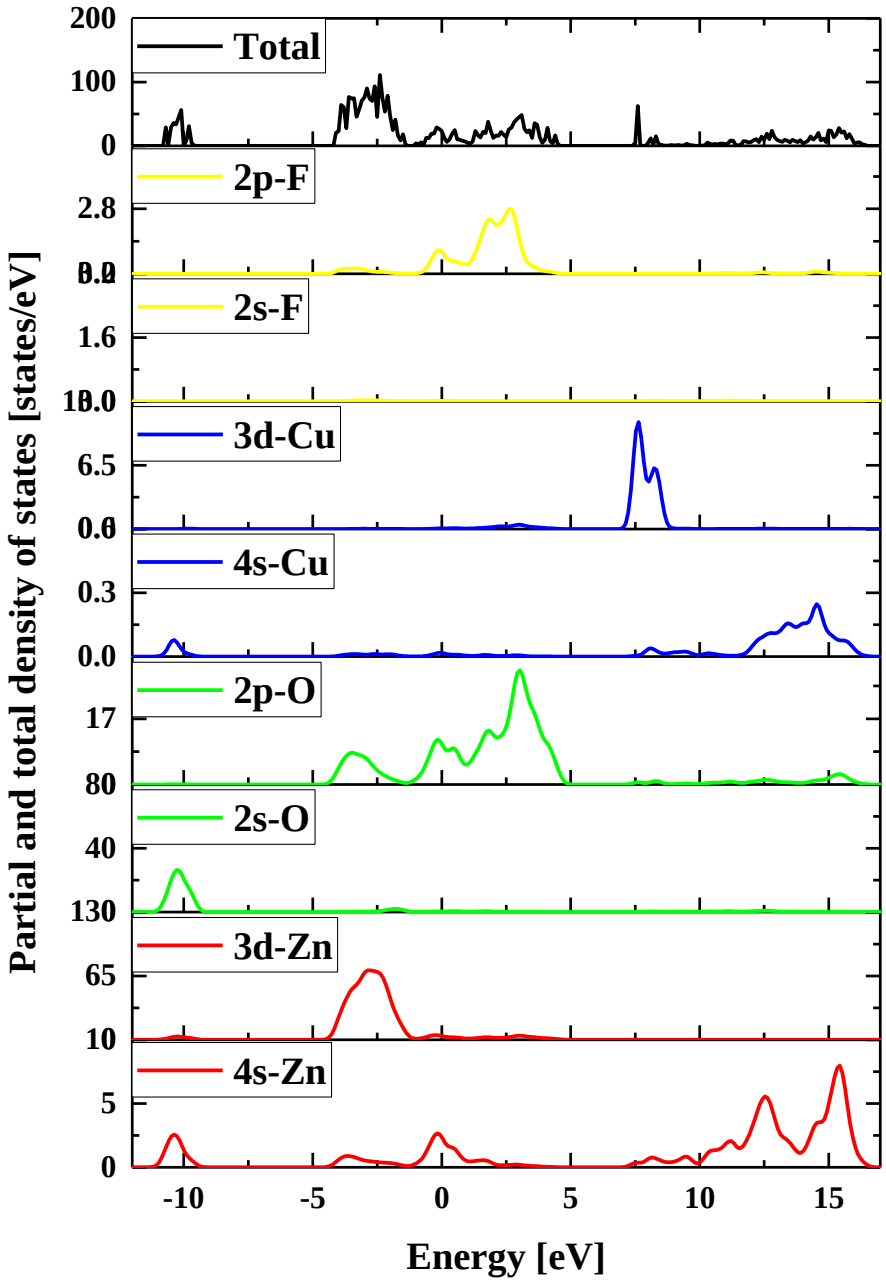

Figure 2-c: Partial density of states of Cu-F codoped ZnO

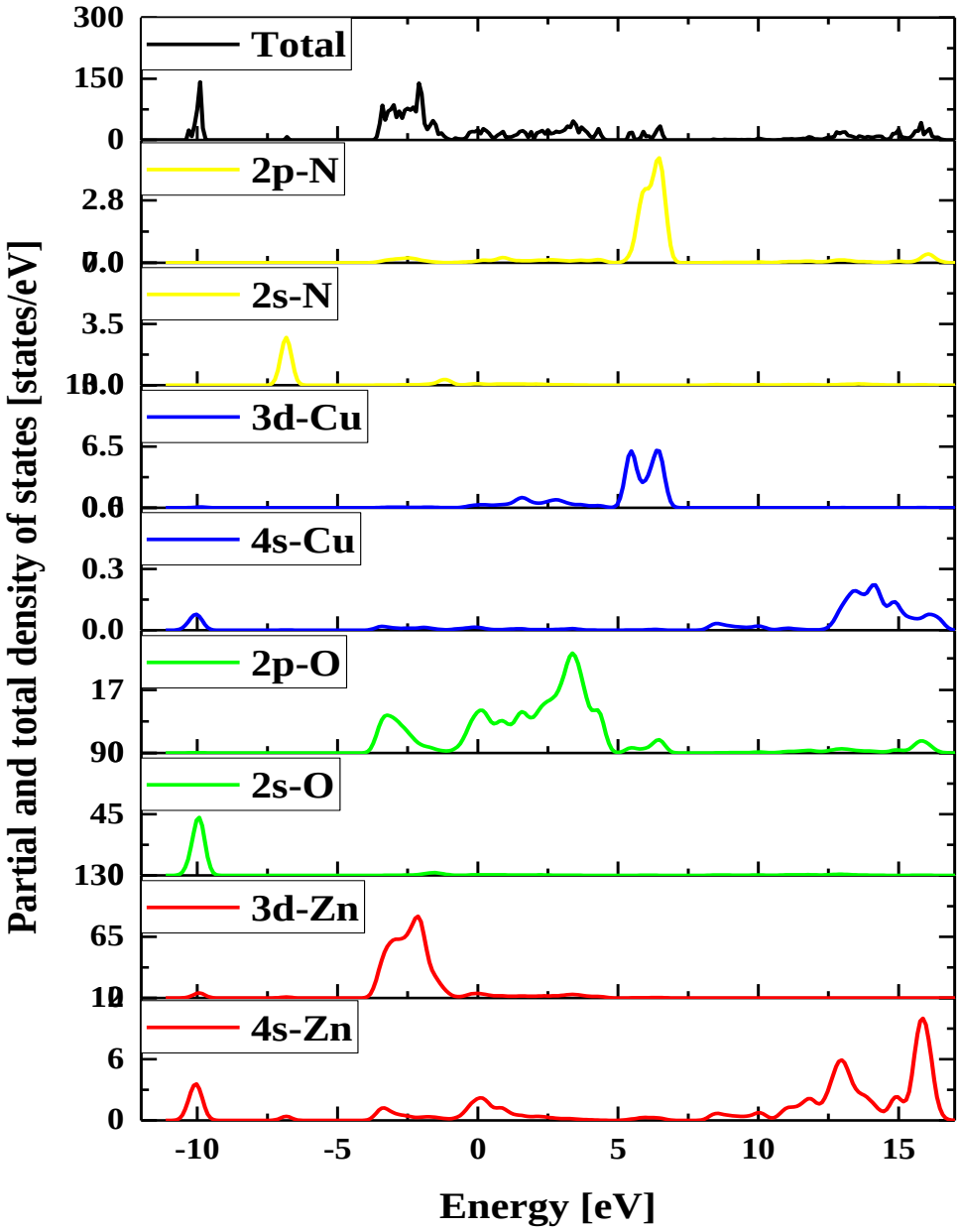

Figure 2-d: Partial density of states of Cu-N codoped ZnO

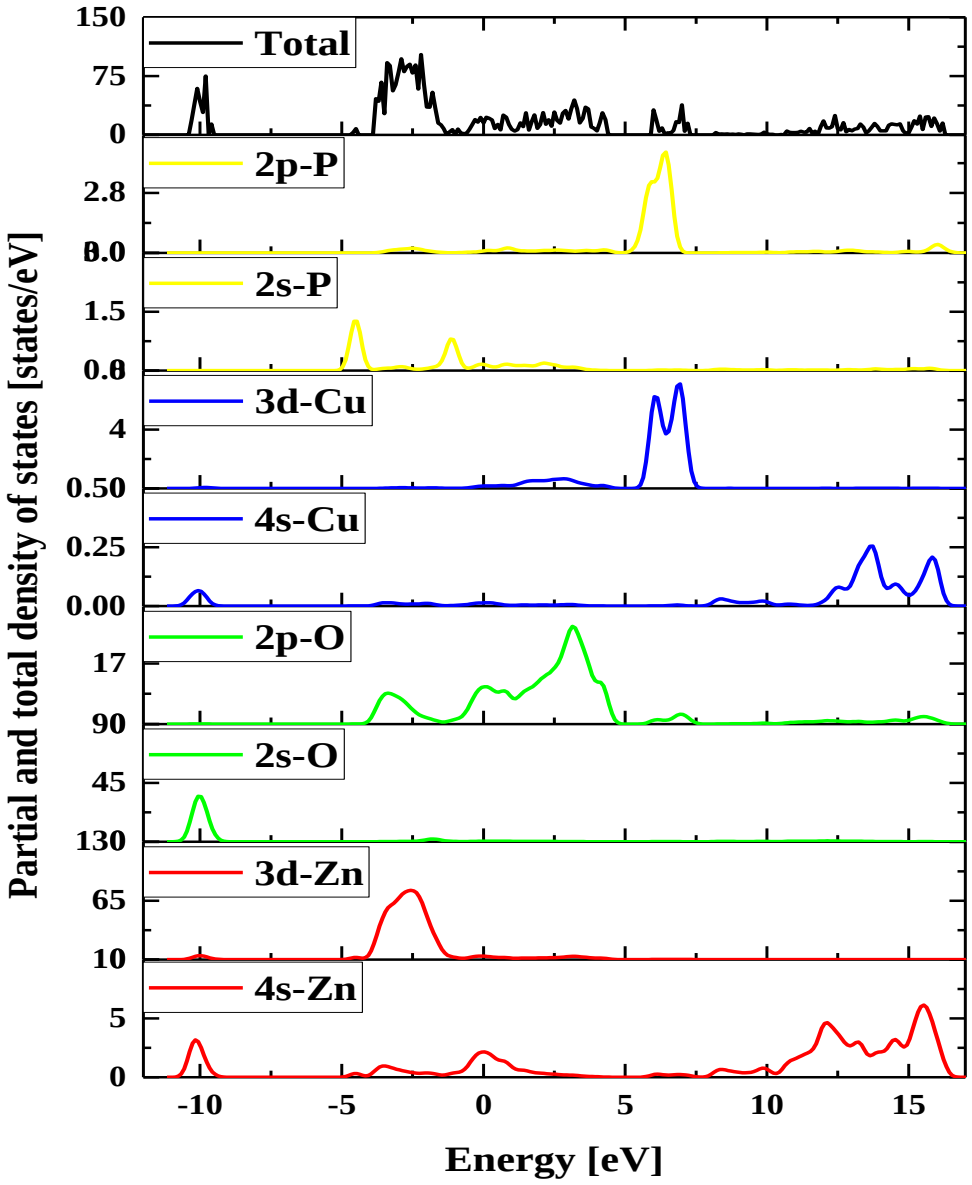

Figure 2-e: Partial density of states of Cu-P codoped ZnO

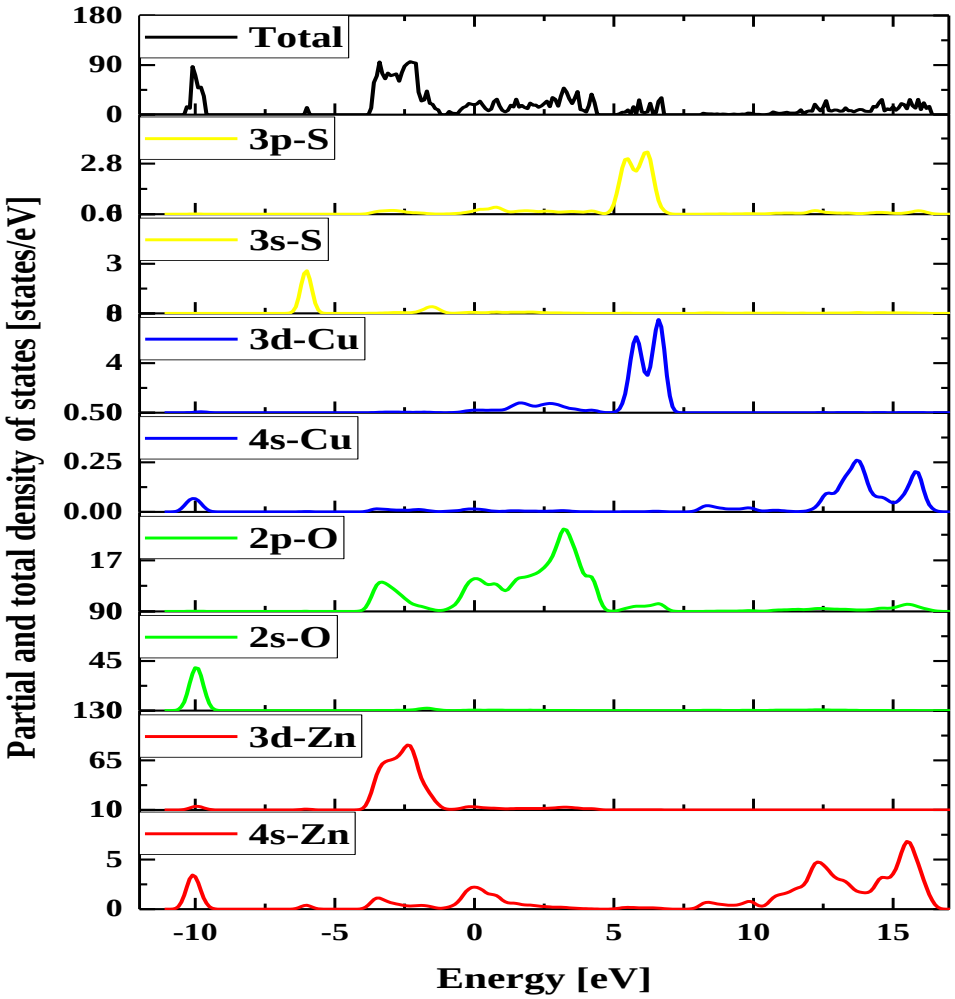

Figure 2-f: Partial density of states of Cu-S codoped ZnO

3.3 Optical Properties

Dielectric properties are important in understanding the optical behavior such as absorption coefficient and transmittance spectrum. In this work, we have calculated the imaginary part of the dielectric function $\varepsilon_i(\omega)$ from the matrix elements of the wave function for occupied and unoccupied states, while the real part of dielectric function $\varepsilon_r(\omega)$ is extracted by using Kramers-Kronig relation. **Fig. 3,** shows the calculated real part of the dielectric function $\varepsilon_r(\omega)$ for pure and co-doped ZnO. The static dielectric constant $\varepsilon(0)$ of pure ZnO is found to be 1.78 which is similar to other reported results. After the incorporation of Cu-(C, N, S and P) we have observed an increase in the static dielectric constant. Similar behavior is obtained in the case of mono-doped ZnO by (S and N) at the O site, which could be due to the presence of the impurity band within the band gap. Furthermore, in the case of Cu-F co-doped ZnO, we report a reduction in the static

dielectric constant. It is to be noted that this sample is a n-type semiconductor and it is well known that when a material turns metallic, the $\varepsilon(0)$ reduces. The imaginary part of dielectric function is presented in **Fig. 4** and it is found to increase after adding the co-doped elements as compared to the pure ZnO. This behavior may be due to the presence of impurity band in the band gap, which increases the photo-generated electrons/holes.

The optical properties need necessary investigation in order to study the suitability of the materials as transparent window for the photovoltaic applications or as an absorber layer. For this reason, we have calculated the transmittance and absorption coefficient in the UV-Visible-Infrared region. **Fig 5,** represents the transmittance of different materials. The average transmittance for pure ZnO in the visible region is around 92% which indicates high transparency in the visible region. This result is already reproduced experimentally indicating that this material is suitable for the application of transparent window in the photovoltaic application. In addition, it is observed that the incorporation of the co-doped elements results in the reduction of the transmittance (absorption increases seen **Fig. 6**). The reduction of transmittance in the visible region can be relate to an increase in the imaginary part of dielectric function due to enhanced density of states at the valence band upon the incorporation of impurities.

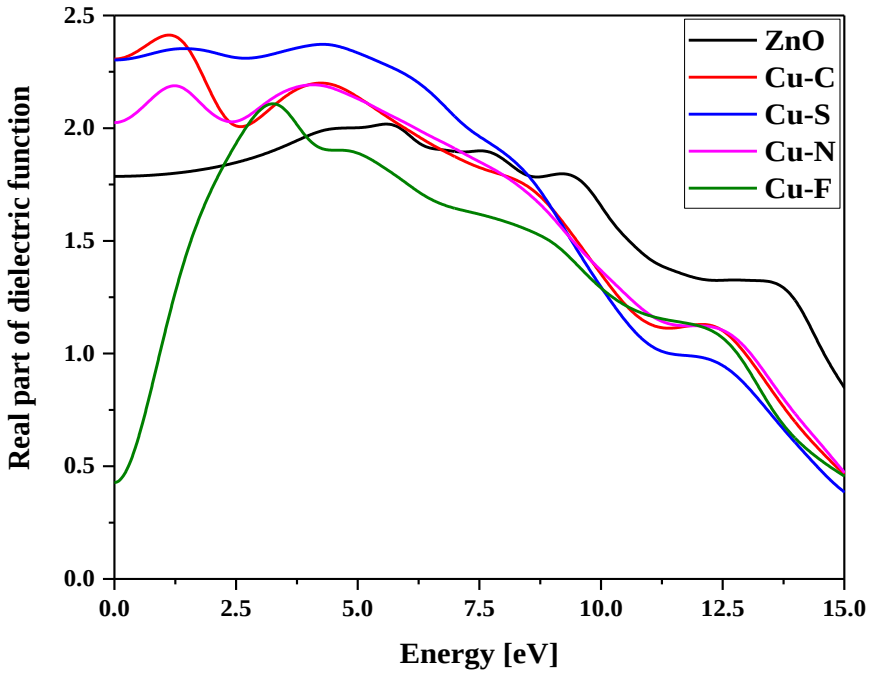

Figure 3: Real part of dielectric function of Cu-X co-doped ZnO

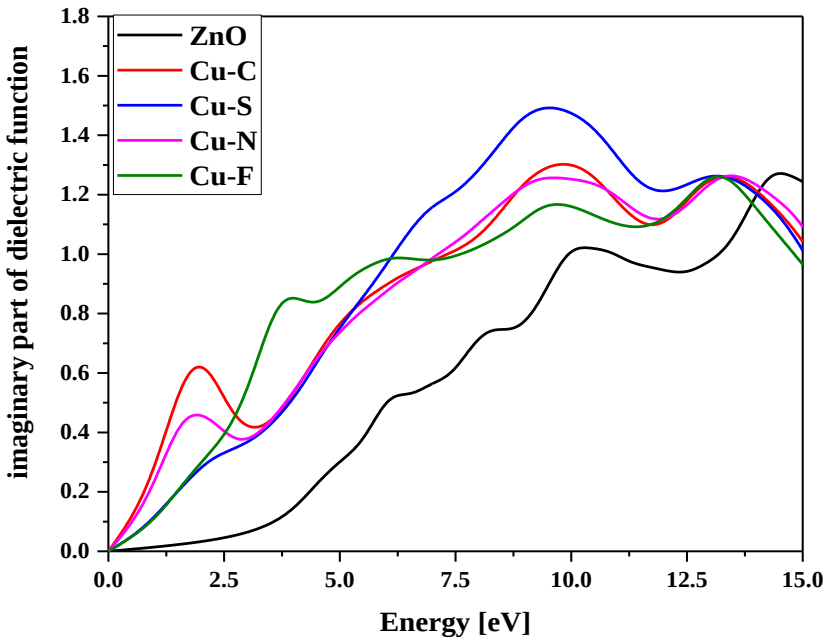

Figure 4: Imaginary part of dielectric function of Cu-X co-doped ZnO

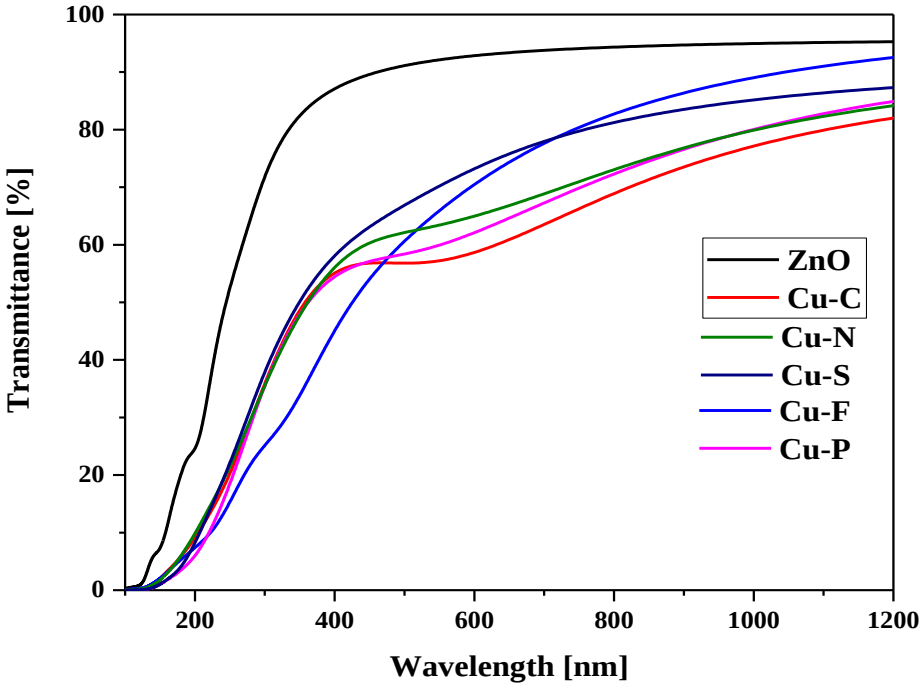

Figure 5: The calculated transmittance spectrum of co-doped ZnO.

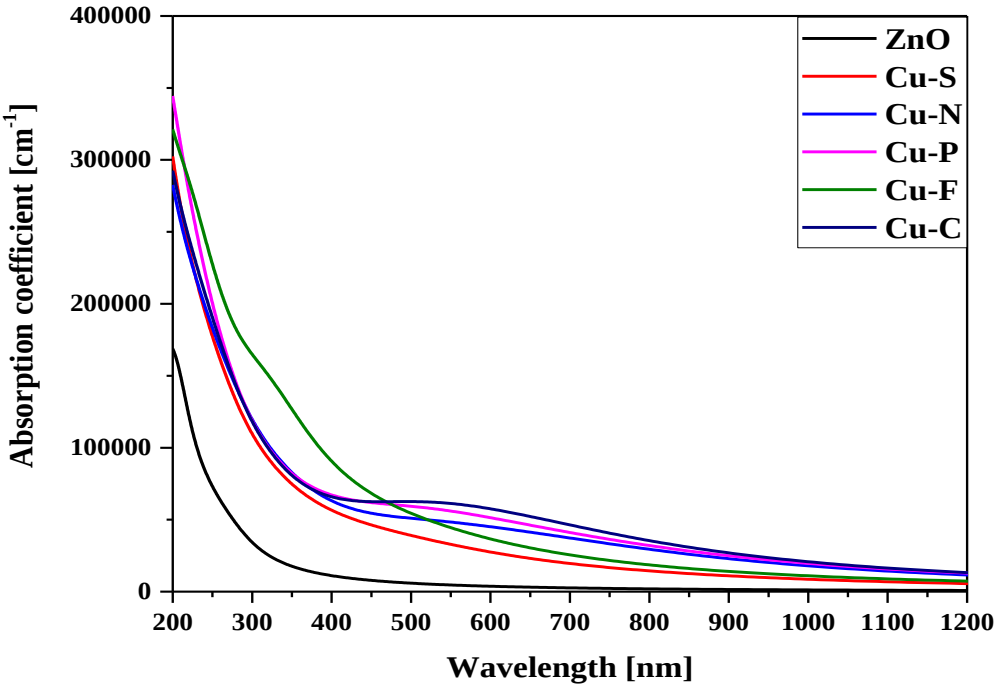

Figure 6: The calculated absorption spectrum of Cu-X co-doped ZnO

3.4 Thermoelectric Properties

It is known that the performance of a photovoltaic device deteriorates with the increasing temperature as the expansion of different layers lead to band offset between these layers, therefore photovoltaic/thermoelectric device is considering a necessary technology device to overcome this challenge. In this work, we have calculated the thermoelectric properties such as charge carrier concentration, electrical conductivity, Seebeck coefficient, thermal conductivity and figure of merit respectively.

Fig 7 represents the charge carrier concentration (c), and a reduction in "c" is found in all the models except Cu-F. This is may be attributes to the compensation of charge carriers by electrons as the conduction in those models occur at the half-filled impurity band as evident from the partial density of states too. Cu-(C, N and S) exhibit charge concentration of the order of 10^{21} cm^{-3} respectively. The electrical conductivity was directly influenced by the charge carrier concentration "c" as can be seen in **Fig 8**. The reduction of "c" is accompanied with an increase in the relaxation time which further increases the electrical conductivity as suggested by the Ong model. This increase in the electrical conductivity indicates that the co-doped materials can be considered as non-degenerate semiconductors. **Fig.9** shows the dependence of the Seebeck coefficient with the co-doped elements as a function of temperature. It is noticed that the Seebeck coefficient increases with the temperature, and the highest Seebeck coefficient is found when ZnO is co-doped with Cu-S. Thermal conductivity is considered to be a crucial parameter in deciding the ZT value. It is preferable to obtain low thermal conductivity in order to have higher efficiency of the thermal conversion energy. **Fig**

10, shows the thermal conductivity behavior of the co-doped elements. It is found that Cu-S co-doped ZnO exhibits the lowest thermal conductivity as it has the highest Seebeck coefficient. However, highest thermal conductivity is obtained for the Cu-F co-doped ZnO. It is to be noted that this material is a n-type semiconductor indicating that the transport is due to electrons at the bottom of the conduction band. Moreover, it is known that the conduction of electrons exhibits lower effective mass as compared to hole, which explains the highest electron thermal conductivity found in the case of Cu-F co-doped ZnO as compared to the rest of materials. **Fig 11,** represents the ZT value of ZnO co-doped and it clearly shows that the Cu-S co-doped ZnO exhibits highest ZT value accompanied by high Seebeck coefficient and low electron thermal conductivity, respectively. Based on these results, co-doping of ZnO with Cu-S seems to be the best choice in order to obtain higher p-type thermoelectric performance.

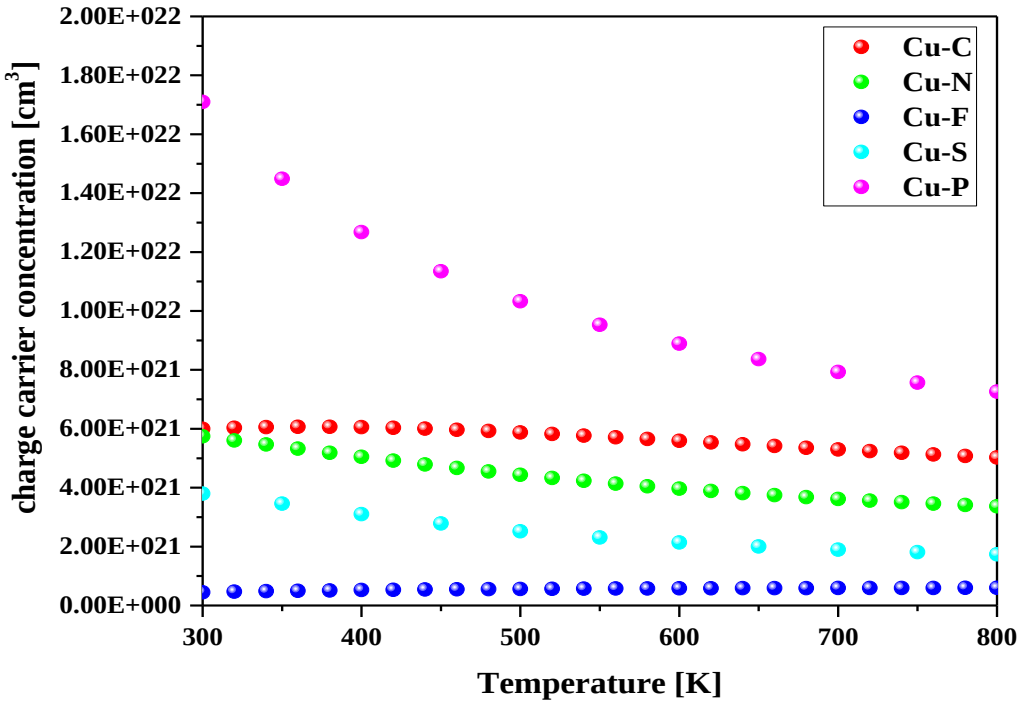

Figure 7: Variation of charge carrier concentration with temperature of co-doped ZnO

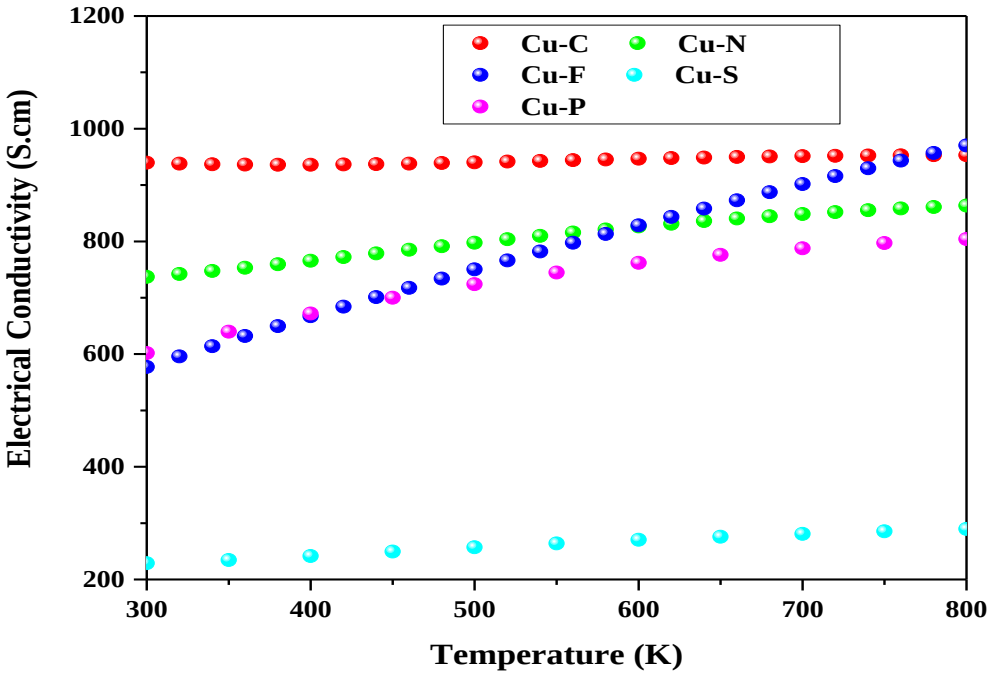

Figure 8: Variation of the electrical conductivity of co-doped ZnO with temperature

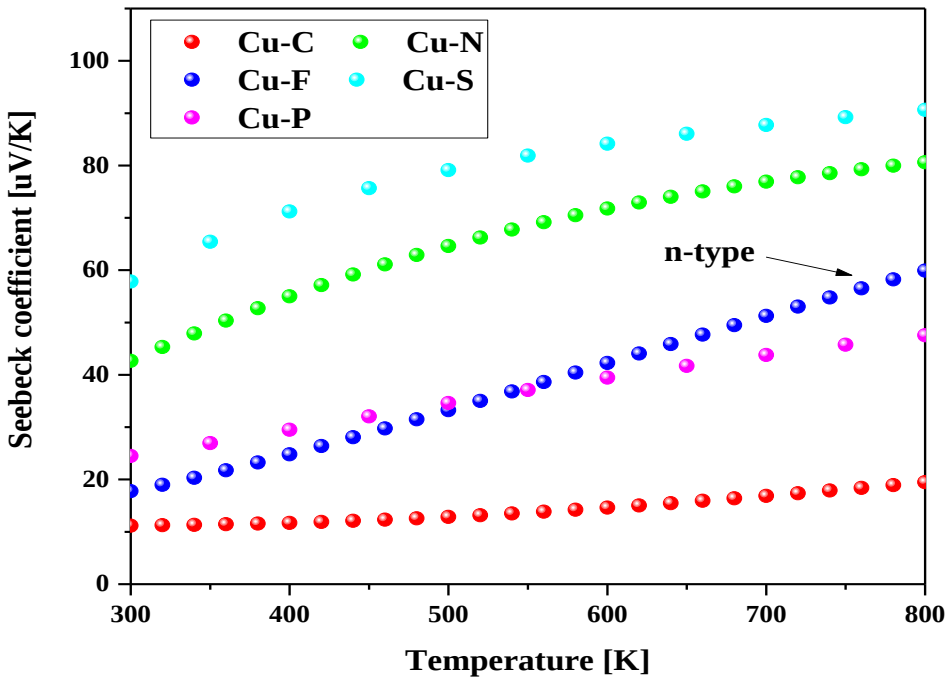

Figure 9: Seebeck coefficient of Cu-X co-doped ZnO at different temperatures

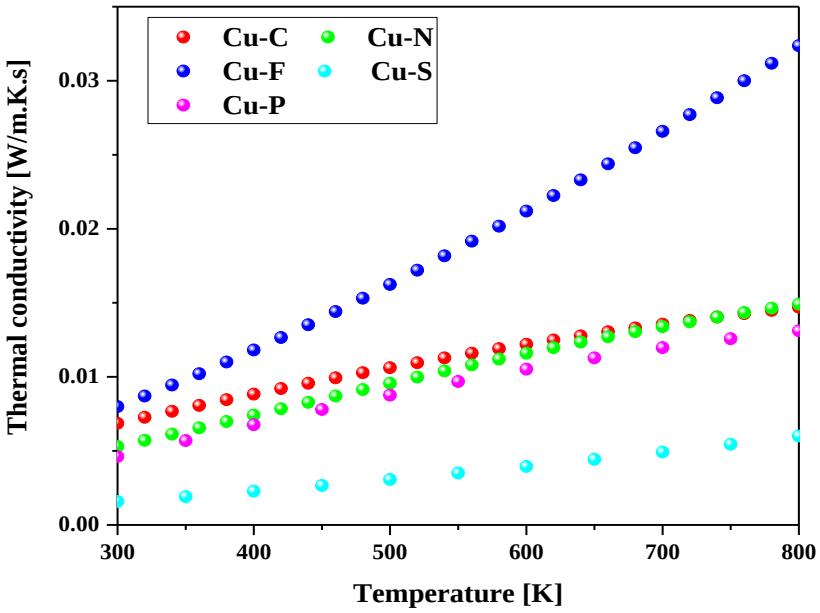

Figure 10: Thermal conductivity of Cu-X co-doped ZnO at different temperatures

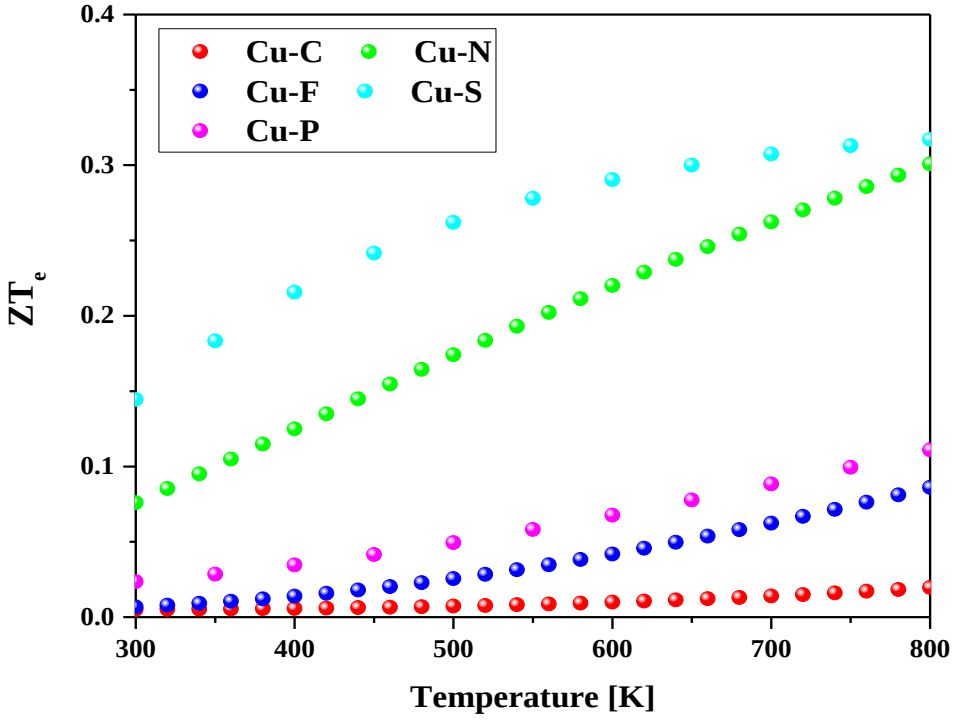

Figure 11: The electronic ZT values of Cu-X co-doped ZnO at different temperatures

4.0 Conclusion

In summary, we have studied the effect of different co-doped elements Cu-(S, N, P, F and C) on the structural, electronic, dielectric, optical and thermoelectric properties of ZnO using first-principles calculation combined with Boltzmann transport equations. The obtained results are in excellent accord with the experimental data. It is found that the Cu-S co-doped ZnO demonstrate high Seebeck coefficient and low electron thermal conductivity. Furthermore, these materials show 70% transparency towards the visible region, making these materials to qualify for high p-type thermoelectric performance.

Acknowledgment

This work is supported by the URAC: 08, the project PPR2: (MESRSFC-CNRST) and also supported by UKM Malaysia Research University Grant (UKM-DIP-2018-008) and completed by National Natural Science Foundation of China (Grant Nos. 51906033 and 51425401), and the Fundamental Research Funds for the Central Universities (Grant Nos. N180902011 and N170908001).

References:

1. F. Abbasim F. Zahedim M. hasan Youse, Optics Comm, (2020) in 126565.
2. H. Ahmoum, G. Li, Y. Piao, S. Liu, R. Gebauer, M. Boughrara, M. S. Su'ait, M. Kerouad, Q. Wang, J Alloy Comp, 854 (2021) 157142.
3. H.-W. Park, K.-B. Chung, J.-S. Park, S. Ji, K. Song, H. Lim, M.-H. Jang, Ceram. Int. 41 (2015) 1641.
4. H. Ahmoum, G. Li, S. Belakry, M. Boughrara, M. S. Su'ait, M. Kerouad, Q. Wang, Mater. Sci. Semic. Proce, (2020) 105530.
5. S. Chenghua, X. Juan, W. Helin, X. Tianning, Y. Bo, L. Yuling, Rev. Sci. Instrum. 82 (2011) 084901.
6. Y. Yang, N. D.Pham, D. Yao, H. Zhu, P. Yarlagadda, H. Wang, Chinese Chemical Letters, 29(8) (2018) 1242.
7. H. Takashima, N. Kikuchi, H.Kawanaka, K. Tonooka, Y. Aiura, Applied Surface Science, 422 (2017) 869.
8. A. El Hichou, S. Diliberto, N. Stein, Surface and Coatings Technology, 270 (2015) 236.
9. H. Ahmoum, M. Boughrara, M.S. Su'ait, S. Chopra, M. Kerouad, Physica B: Condensed Matter, 560 (2019) 28.
10. G. Li, H. Ahmoum, S. Liu, S. Liu, M. S. Su'ait, M. Boughrara, M. Kerouad, Q. Wang, Physica B: Condensed Matter, 562 (2019) 67.
11. H. Ahmoum, M. Boughrara, M. S. Su'ait, M. Kerouad, Chemical Physics Letters, 719 (2019) 45.
12. Y. Gao, G. Li, Z. Wang, S. Liu, Q. Wang, Applied Surface Science, 416 (2017) 521.
13. Q. Hou, S. Sha, Materials Today Communications, 24 (2020) 101063.
14. B. K. Singh, S. Tripathi, Journal of Luminescence, 198 (2018) 427.
15. Z. Ye, H. He, L. Jiang, Nano Energy, 52 (2018) 527.
16. F. Ghahramanifard, A. Rouhollahi, O. Fazlolahzadeh, Superlattices and Microstructures, 114 (2018) 1.
17. K. Lamhal, R. Hayn, A. Boukortt, S. Meskine, L. Abbes, A. Zaoui, Physica B: Condensed Matter, 545 (2018) 491.
18. M. P. Lu, M. Y. Lu, L. J. Chen, Nano Energy, 1(2) (2012) 247.

19. W. Li, C. Kong, G. Qin, H. Ruan, L. Fang, Journal of Alloys and Compounds, 609 (2014) 173.
20. W. W. Liu, C. L. Liu, X. B. Chen, J. H. Lu, H. X. Chen, Z. Z Miao, Physics Letters A, 384(8) (2020) 126172.
21. H. B. Ruan, C. Y. Kong, G. P. Qin, W. J. Li, T. Y. Yang, F. Wu, L. Fang, Journal of Magnetism and Magnetic Materials,369 (2014) 219.
22. Y.Zhao, M. Zhou, Z. Lv, Z. Li, J. Huang, X. Liang, J. Min, Materials Science in Semiconductor Processing, 14 (2011) 257.
23. H. Ahmoum, M. S. Su'ait, G. Li, S. Chopra, M. Boughrara, Q. Wang, M. Kerouad, D. P. Rai, Indian J. Phys. (2020), https://doi.org/10.1007/s12648-020-01698-3.
24. I. Jellal, H. Ahmoum, Y. Khaaissa, K. Nouneh, M. Boughrara, M. Fahoume, S. Chopra, J. Naja, Applied Physics A,125 (2019) 650.
25. H. Ahmoum, M. Boughrara, M. Kerouad, P. Chelvanathan, K. Sopian, M.S. Su'ait, L. T. Khoon, B. Jia, G. Li,Jurnal Kejuruteraan, 1 (3) (2018) 15.
26. Z. Wu, J. Wu, Y. Li, G. Li, Ceramics International, 46(13) (2020) 21617.
27. S. Liu, G. Li, M. Lan,Y. Piao, Y. Zhang, Q. Wang, Current Applied Physics, 20(3) (2020) 400.
28. G. Li, L. Xiao, S. Liu, H. Wang, Y. Gao, Q. Wang, Journal of the European Ceramic Society, 38(4) (2018) 1608.
29. J. C. Fan, K. M. Sreekanth, Z. Xie, S. L. Chang, K. V. Rao, Prog. Mater. Sci. 58 (6) (2013) 874.
30. P. Giannozzi, et al., A modular and open-source software project for quantum simulations of materials, J. Phys. Condens. Matter 21 (2009) 395502.
31. J.P. Perdew, K. Burke, M. Ernzerhof, Phys. Rev. Lett. 77 (1996) 3865.
32. H.J. Monkhorst, J.D. Pack, Phys. Rev. B 13 (1976) 5188.
33. K. Meziane, A. El Hichou, A. El Hamidi, M. Mansori, A. Liba, A. Almaggoussi, Superlattice. Microst. 93 (2016) 297–302.
34. M. Khuili, N. Fazouan, H.A. El Makarim, G. El Halani, E.H. Atmani, J. Alloy. Comp. 688 (2016) 368.
35. W. Yu, J. Zhang, T. Peng, Appl. Catal. B Environ. 181 (2016) 220.